







Kinetics Analysis of Crystal Violet Adsorption from Aqueous Solution onto Flamboyant Pod Biochar

Azeez G. Akinyemi^{1,2*} , Abass O. Alade^{1,2,3} , Akeem O. Arinkoola¹ ,
Shukurat B. Olabiyi¹ .

¹Department of Chemical Engineering, Ladoké Akintola University of Technology, Ogbomosó, Nigeria

²Bioenvironmental, Water and Engineering Research Group (BWERG), Ladoké Akintola University of Technology, Ogbomosó, Nigeria

³Science and Engineering Research Group (SAERG), Ladoké Akintola University of Technology, Ogbomosó, Nigeria

Abstract: The increasing presence of persistent synthetic dyes, like crystal violet (CV), in wastewater poses a significant threat to aquatic ecosystems and human health due to its genotoxicity and carcinogenicity. Biochar derived from agricultural waste offers a promising, cost-effective, and eco-friendly approach for dye removal. This study explores the potential of flamboyant pod biochar (FPB) as a novel and sustainable adsorbent for CV removal. FPB offers a unique advantage as it utilizes readily available flamboyant pod waste, promoting waste valorization and a cost-effective approach. FPB was synthesized through a simple process involving milling, sun-drying, and pyrolyzing flamboyant pod waste at 300 °C. Batch adsorption experiments were conducted to evaluate the influence of contact time and initial dye concentration on removal efficiency. Kinetic modeling using pseudo-first-order and pseudo-second-order models explored the underlying mechanisms governing the adsorption process. The pseudo-second-order kinetic model exhibited a superior fit ($R^2 > 0.87$) compared to the pseudo-first-order model, suggesting a chemisorption mechanism governing the adsorption process. These findings demonstrate the potential of FPB as a low-cost, sustainable adsorbent for CV removal from wastewater.

Keywords: Adsorption, Biochar, Crystal Violet, Error Analysis, Kinetic Model.

Submitted: January 14, 2024. **Accepted:** May 06, 2024.

Cite this: Akinyemi, A. G., Alade, A. O., Arinkoola, A. O., & Olabiyi, S. B. (2024). Kinetics Analysis of Crystal Violet Adsorption from Aqueous Solution onto Flamboyant Pod Biochar. *Journal of the Turkish Chemical Society, Section B: Chemical Engineering*, 7(2), 105-122. <https://doi.org/10.58692/jotcsb.1414940>,

*Corresponding author. E-mail: azeezakinyemi61@gmail.com Tel: +2349060267570.

1. INTRODUCTION

Dyes, a ubiquitous group of synthetic aromatic compounds, find application across a vast spectrum of industries, including textiles, food, and pharmaceuticals. However, their recalcitrance towards biodegradation presents a significant environmental challenge. Effluent from the textile industry, a major source of dye contamination, is estimated to contain 10-20% of unused dyes. Adsorption has emerged as a promising strategy for the removal of these pollutants from wastewater due to its high efficiency, reusability, and

diverse range of adsorbent materials (Chahinez et al., 2020; Zamouche et al., 2020).

Crystal violet (CV), a commonly used cationic dye, was selected for this study due to its hazardous nature and strong adsorption properties. Cationic dyes like CV pose a greater threat to human health and the environment compared to their anionic counterparts. This is attributed to their strong affinity for negatively charged cell membranes. This electrostatic attraction allows CV to readily interact with and penetrate living cells, accumulating within

the cytoplasm (Zamouche *et al.*, 2020). CV exhibits cytotoxicity and genotoxicity, including mutagenic and carcinogenic properties (Abbasi *et al.*, 2020). Therefore, developing efficient methods for CV removal from wastewater is crucial.

Delonix regia pods, commonly known as flamboyant pods or flame tree pods, present a promising renewable feedstock for biochar production. These large, lignocellulosic pods are a byproduct of the flamboyant tree (*Delonix regia*), a popular ornamental species cultivated throughout tropical and subtropical regions. Following seed dispersal, the pods naturally detach from the tree and accumulate as a significant component of agricultural waste. Fortunately, flamboyant pods possess several characteristics that make them ideal biochar feedstock. Their abundance, cellulosic composition, and ease of collection and processing after falling from the tree contribute to their suitability. Moreover, utilizing flamboyant pods for biochar creation not only addresses agricultural waste management but also transforms this waste into a valuable product for environmental applications, promoting a sustainable waste valorization approach.

Biochar has emerged as a promising adsorbent for dye remediation due to its exceptional capacity. This stems from its high surface area, offering a multitude of binding sites for dye molecules, and the presence of diverse functional groups on its surface that can interact favorably with dyes. While traditional methods often boast high efficacy, their economic feasibility can be hindered by the vast array of dye structures. The adsorption capacity and specific interaction mechanisms between biochar and dye pollutants are influenced by a complex interplay of factors. These include the inherent characteristics of the dye itself, the properties of the biochar (such as surface chemistry and porosity), environmental conditions (pH, ionic strength), and even the aging process of the biochar (Vyavahare *et al.*, 2019). Understanding the impact of these key factors is crucial for optimizing biochar's application in dye removal.

In recent years, adsorption has emerged as a preferred method for dye removal from wastewater due to several advantages, including high efficiency, ease of operation, a vast array of applicable adsorbent materials, and cost-effectiveness (Loulidi *et al.*, 2020).

However, optimizing adsorption processes for maximum dye removal efficiency necessitates a thorough understanding of the various influencing parameters and their impact on adsorption capacity. Traditional optimization techniques often rely on a substantial number of experiments, which can be both expensive and time-consuming (Rosly *et al.*, 2021). Furthermore, these methods might not adequately capture the intricate interactions between process variables and their combined effects on the adsorption capacity (Rosly *et al.*, 2021).

This study addresses these limitations by investigating flamboyant pod biochar (FPB) as a novel, sustainable adsorbent for crystal violet removal. We explore the efficacy of FPB by examining the influence of key adsorption parameters such as dye concentration, contact time, and FPB dosage. Furthermore, equilibrium isotherms and error analysis are employed to elucidate the mechanism and correlation governing the adsorption process.

2. MATERIAL AND METHODS

2.1. Biochar Synthesis from Flamboyant Pod

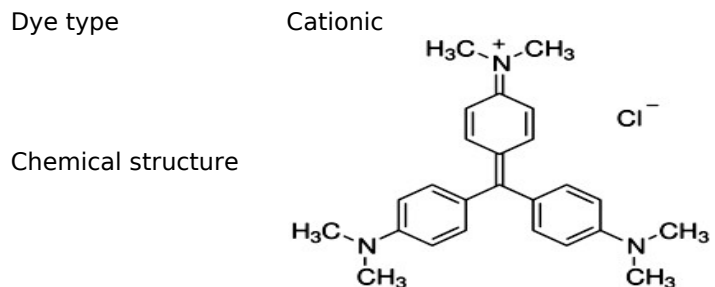
The acquired flamboyant pod sample was washed with distilled water to remove surface impurities, sun-dried for 48 hours to reduce moisture content, milled with PMG-100, power mortar grinder, and sieved using a 2 mm mesh sieve size to obtain uniform particle size. The resulting flamboyant pod sample was calcined at temperature (300 °C), particle size (2 mm), flamboyant pod moisture (10 %), and pyrolysis duration (30 minutes) in a muffle furnace to produce flamboyant pod biochar, referred to as FPB (Barber *et al.*, 2018).

2.2. Preparation of Adsorbate Solution

The Crystal Violet (CV) dye (chemical formula = $C_{25}H_{30}N_3Cl$, solubility in water 16 g/L at 25 °C, Molecular weight = 407.98 g/mol) with a purity of 99% was used in this study (structure shown in Table 1). A stock solution of 1000 mg/L CV was prepared by dissolving 1 g of the dye in 1 L of distilled water in a volumetric flask. The stock solution was stored in a dark environment to avoid depolarization. All working solutions with desired concentrations were prepared by diluting the stock solution with distilled water according to standard methods (APHA 1995).

Table 1: Characteristics and chemical properties of crystal violet.

Name	Crystal Violet
Chemical formula	$C_{25}H_{30}N_3Cl$
Molecular weight	407.98 g/mol
λ_{max} (nm)	590 nm



2.3 Batch Adsorption Experiment

All experiments were conducted in triplicate, and the reported values represent averages with associated standard deviations. Initial optimization experiments established the optimal range for initial dye concentration (50-250 mg/L) and contact time (10-225 minutes). For the adsorption experiments, 100 mL of dye solution with an initial concentration of 50 mg/L was added to 250 mL conical flask along with a 1 g of FPB. The mixture was agitated on a shaker (Bioshaker BR-23FH) at 150 rpm for the desired contact time (10-225 minutes). After agitation, the residual concentration of the dye solution were obtained using a UV-visible spectrophotometer, measuring absorbance at the maximum wavelength of CV ($\lambda_{max} = 590 \text{ nm}$).

$$\text{Removal Efficiency (\%)} (\text{RE}) = \frac{C_0 - C_e}{C_0} \times 100 \quad (1)$$

$$\text{Adsorption Capacity}_{(mg/g)} @ \text{equilibrium} (q_e) = (C_0 - C_e) \frac{M}{V} \quad (2)$$

$$\text{Adsorption Capacity}_{(mg/g)} @ \text{any time} (q_t) = (C_0 - C_t) \frac{M}{V} \quad (3)$$

Where C_0 and C_e are the initial and final concentration of the crystal violet and m and v is the mass of the biochar and volume of

the adsorbate utilized, while q_e and q_t are adsorption capacity (mg/g) at equilibrium and any time, respectively.

2.4. Analysis of Experimental Data

2.4.1. Adsorption kinetic model

Adsorption kinetics plays a pivotal role in determining the pace at which a solute is taken up, while influencing the duration of its interaction at the solid-solution interface. Therefore, it is essential to comprehend the reaction mechanism governing the sorption process for the effective design of sorption treatment facilities. If not adequately comprehended, the adsorption kinetics could present significant challenges in the development of treatment systems incorporating adsorbents. Furthermore, it serves as a tool to identify the rate-limiting step within an adsorption process. The insights derived from adsorption kinetics are invaluable to industry operators and planners, offering crucial guidance for the appropriate treatment of contaminated wastewater through adsorption. In practical or industrial settings, the rapid adsorption of solutes in an adsorption system is highly desirable. Kinetic parameters aid in predicting the adsorption rate and equilibrium time, providing essential information for the design and modeling of adsorption processes. The specific adsorption kinetics examined in this research are detailed below.

Table 2: Linear and non-linear forms of adsorption kinetic models (8).

Models	Non-linear	Equation
Zeroth order	NA	$q_t = k_0 t + q_0$
First order	NA	$\ln q_t = k_1 t + \ln q_0$
Second order	NA	$\frac{1}{q_t} = k_2 t + \frac{1}{q_0}$
Third order	NA	$\frac{1}{q_t^2} = k_3 t + q_0^2$
Pseudo-first order		
Type 1	$q_t = q_e (1 - e^{-k_1 t})$	$\log(q_e - q_t) - \log(q_e) = \frac{-k_1 t}{2.303}$

Type 2

Type 3

$$c_t = c_o e^{-k_1 t}$$

Type 4

$$\ln(q_e - q_t) - \ln(q_e) = -k_1 t$$

$$\ln\left(\frac{c_t}{c_o}\right) = -k_1 t$$

$$\ln\left(1 - \frac{c_o - c_t}{c_o - c_e}\right) = -k_1 t$$

Pseudo Second Order

Type 1

$$\frac{1}{q_t} = \frac{1}{k_2 q_e^2} + \frac{t}{q_e}$$

Type 2

$$\frac{1}{q_t} = \frac{1}{k_2 q_e^2} \frac{1}{t} + \frac{1}{q_e}$$

Type 3

$$\left(\frac{1}{q_t} - \frac{1}{q_e}\right) q_e^2 = \frac{1}{k_2 t}$$

Type 4

$$q_t = q_e \left[1 - \frac{1}{1 + k_2 t} \right]$$

$$q_t = q_e - \left(\frac{1}{k_2 q_e}\right) \frac{q_t}{t}$$

Type 5

$$(q_t - q_e) q_e = -\left(\frac{q_t}{k_2 t}\right)$$

Type 6

$$\frac{q_t}{t} = k_2 q_e^2 - k_2 q_e q_t$$

Type 7

$$\frac{1}{q_e - q_t} - \frac{1}{q_e} = k_2 t$$

Type 8

$$\frac{1}{t} = k_2 q_e^2 \left(\frac{1}{q_t}\right) - k_2 q_e$$

Type 9

$$\frac{q_e}{q_e - q_t} - 1 = k_2 t$$

Type 10

$$\frac{\Theta}{1 - \Theta} = k_2 t$$

Type 11

$$C_t - \frac{1}{C_0} = k_2 t$$

Type 12

$$\frac{1}{C_t} - \frac{1}{C_0} = k_2 t$$

Type 13

$$\frac{1}{C_0 - C_t} = k_2 t + b$$

Pseudo-third order

$$q_t = q_e \left[1 - \frac{1}{(1 + 2k_3 t)^{\frac{1}{2}}} \right]$$

Esquivel kinetic model

Type 1

$$q_t = q_e \left(\frac{t}{t + K_E} \right)$$

Type 2

$$\frac{1}{q_t} = \frac{K_E}{q_e t} + \frac{1}{q_e}$$

$$\left(\frac{1}{q_t} - \frac{1}{q_e}\right) q_e = \frac{K_E}{t}$$

Elovich kinetic model

Type 1

$$q_t = k_5 \ln(k_5 k_{eq}) + k_5 (\ln t)$$

Type 2	$q_t = \frac{-k_4}{k_5} t e^{-k_1 q_t}$	$q_t = \frac{1}{k_6} \ln(k_6 k_7) + \frac{1}{k_6} \ln t$
Avrami	$q_t = q_e - q_e \exp(-k t^n)$	$\ln \left(\ln \left(\frac{q_e}{q_e - q_t} \right) \right) = n \ln k + n \ln t$

2.4.2 Statistical Error Analysis

Over the years, error functions have found utility in the selection of the appropriate adsorption model. Their primary utility lies in quantifying the dispersion of the adsorbent, facilitating a rigorous quantitative analysis of the data, and, most significantly, confirming the consistency of the experimental results, which underpin the construction of the

adsorption model (Benmaamar *et al.*, 2017). In this process, the most suitable equation is derived by employing established special functions to quantify the error deviation between the experimentally observed data and the estimated values. The mathematical equations for these error functions are presented in Table 3.

Table 3: Mathematical equations of error analysis function.

Error function	Equation	Reference
Sum square error	$SSE = \sum_{i=1}^n (q_{\text{exp}} - q_{\text{obs}})^2$	(Batool <i>et al.</i> , 2018)
Hybrid function fractional error	$HYBRID = \frac{100}{p-n} \sum_{i=1}^p \left[\frac{(q_{e,\text{exp}} - q_{e,\text{cal}})^2}{q_{e,\text{exp}}} \right]$	(Sivarajasekar & Baskar, 2019)
Marquardt's percent standard deviation (MPSD)	$MPSD = 100 \sqrt{\frac{1}{n-p} \sum_{i=1}^n \left(1 - \frac{q_{e,\text{cal}}}{q_{e,\text{obs}}} \right)^2}$	(Olafadehan, 2021)
Sum of normalized errors	$SNE = \sum_{i=1}^n \frac{f_i}{f_{i,\text{max}}}$	(Adekunbi <i>et al.</i> , 2020)
Sum of absolute errors	$SAE = \sum_{i=1}^n q_{\text{exp}} - q_{\text{obs}} $	(Shojaei <i>et al.</i> , 2019)
Residual Sum of Squares	$RSS = \sum_{i=1}^n q_{\text{exp}} - q_{\text{obs}} ^2$	(Elmorsi <i>et al.</i> , 2022)
Nonlinear chi-square test	$X^2 = \sum_{i=1}^n \frac{(q_{e,\text{obs}} - q_{e,\text{cal}})^2}{q_{e,\text{obs}}}$	(Hami <i>et al.</i> , 2019)
Coefficient of determination (R2)	$R^2 = 1 - \frac{\sum_{i=1}^n (q_{e,\text{exp}} - q_{e,\text{cal}})^2}{\sum_{i=1}^n (q_{e,\text{cal}} - q_{e,\text{exp}})^2}$	(Popoola, 2019)
Average relative error (ARE)	$ARE = \frac{1}{n} \sum_{i=1}^n \left \frac{q_{e,\text{obs}} - q_{e,\text{cal}}}{q_{e,\text{obs}}} \right $	(Adekunbi <i>et al.</i> , 2020)
Standard deviation of relative error (SRE)	$SRE = \sqrt{\frac{1}{n} \sum_{i=1}^n [(q_{e,\text{obs}} - q_{e,\text{cal}}) - ARE]^2}$	(Popoola, 2019)
Residual Root Mean Squared Error (RMSE)	$RMSE = \frac{1}{n-2} \sqrt{\sum_{i=1}^n (q_{e,\text{obs}} - q_{e,\text{cal}})^2}$	(Elmorsi <i>et al.</i> , 2022)
ARED	$ARED = \frac{100}{n} \sum_{i=1}^n \left \frac{q_{e,\text{obs}} - q_{e,\text{cal}}}{q_{e,\text{obs}}} \right $	(Olafadehan, 2021)

$$\begin{aligned}
 \text{ARS} &= \sqrt{\frac{\sum_{i=1}^n \left[\frac{q_{e,obs} - q_{e,cal}}{q_{e,obs}} \right]^2}{n-1}} && \text{(Hami et al., 2019)} \\
 \text{MPSED} &= \sqrt{\frac{\sum_{i=1}^n \left[\frac{q_{e,obs} - q_{e,cal}}{q_{e,obs}} \right]^2}{n-p}} && \text{(Elmorsi et al., 2022)} \\
 \Delta q (\%) = 100 * \text{ARS} &= 100 \sqrt{\frac{\sum_{i=1}^n \left[\frac{q_{e,obs} - q_{e,cal}}{q_{e,obs}} \right]^2}{n-1}} && \text{(Shojaei et al., 2019)}
 \end{aligned}$$

In this study, several key parameters are employed to evaluate and analyze the adsorption of crystal violet onto FPB. The number of experimental data points, denoted as "n," plays a crucial role in shaping the analysis. Additionally, "q_{cal}" represents the calculated amount of crystal violet adsorbed onto FPB, while "q_{obs}" (or "q_{exp}") signifies the experimentally observed data. The variable "p" indicates the number of parameters utilized within each kinetic model, reflecting the model's complexity. Further, various metrics are utilized to assess the quality and accuracy of the analysis, including ARED, ARE, ARS, and the dimensionless parameter "HYBRID." Additionally, parameters such as SNE, MPSD, MPSED, SAE, SSE, and q(%) are all examples of normalized error metrics used to rigorously assess the adsorption process.

3. RESULTS AND DISCUSSION

3.1. Effect of Contact Time

The contact time has a major impact on the performance of the adsorption process. It helps to determine how long it takes for CV adsorption on FPB to attain equilibrium. An initial concentration of 100 mg/L, continual agitation of 150 rpm, a dose of 1 g of FPB, room temperature, and contact times between 30 and 225 minutes were applied in this experiment. Three steps of adsorption are visible in the result. Adsorption proceeds fast at stage 1 of the process, and dye molecules enter the process's huge pores on the adsorbent's surface instantly shortly. Stage 2 contains a slower intra-particle diffusion process when dye molecules penetrate the tiny pores of the adsorbent, and stage 3 is when equilibrium is attained. Further adsorption was minimal as a function of contact time after establishing equilibrium (Çoruh & Geyikçi, 2012). The FPB reaches saturation in roughly 66 minutes and has an adsorption capacity and removal efficiency that improve with time. There are several accessible active sites on the FPB adsorbent surface, which contributes to the first

increase in the rate of adsorption capacity. In contrast to the sluggish CV adsorption, which was created by the saturation of the binding sites, the slow adsorption of dye ions was caused by the repulsive forces between the dye ions and the ions already adsorbed on the adsorbent (Lairini et al., 2017).

The effect of contact time on CV adsorption by FPB was investigated. Experiments employed an initial CV concentration of 100 mg/L, continuous agitation at 150 rpm, a 1 g FPB dose, and room temperature, with contact times varying from 30 to 225 minutes. The results revealed a three-stage adsorption process. Stage 1 exhibited a rapid initial uptake as CV molecules readily occupied the abundant pores on the FPB surface, leading to a significant increase in both adsorption capacity and removal efficiency due to the presence of numerous active sites. Stage 2 involved a slower intra-particle diffusion process where dye molecules penetrated the smaller pores of the FPB, resulting in continued adsorption at a slower rate. Finally, Stage 3 represented the achievement of equilibrium, where further adsorption became minimal with increasing contact time (Çoruh & Geyikçi, 2012). FPB reached saturation around 66 minutes. This three-stage process highlights the interplay between available active sites and repulsive forces. The initial rapid adsorption and subsequent slowdown can be attributed to the depletion of active sites and the development of repulsive forces between incoming CV molecules and those already adsorbed on the FPB (Lairini et al., 2017).

3.2. Pareto Analysis of the Effect of Time on QE and RE

The Pareto analysis (Equation 4), also known as the 80/20 rule, is a valuable tool for identifying the factors with the most significant influence on a process. In this study, we employed Pareto analysis to assess the relative importance of contact time on the adsorption capacity (QE) and

removal efficiency (RE) of CV by FPB (Zarei *et al.*, 2010):

$$P_i(\%) = \left[\frac{(b_i^2)}{\sum b_i^2} \right] \times 100 \quad (4)$$

The Pareto effect of each item in Equation 4 is represented in P_i , whereas B_i shows the regression coefficients from the regression equation in terms of coded values. As shown

in Figure 1, the contact time between 0 and 45 minutes has the greatest impact on the adsorption capacity and the removal efficiency of CV dye by the FPB adsorbent, with the first 45 minutes accounting for about 80% of the adsorbent's activity in the removal of dye, compared to the remaining of the 225 minutes, which account for only 20%. The bulk of CV dye adsorption happened within the first five minutes and over 80% of the dye was absorbed during the (30 mins) rapid adsorption phase.

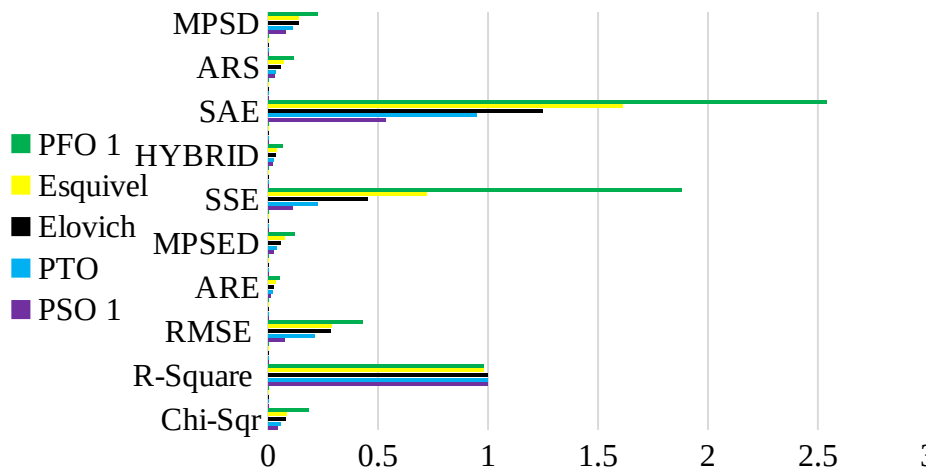
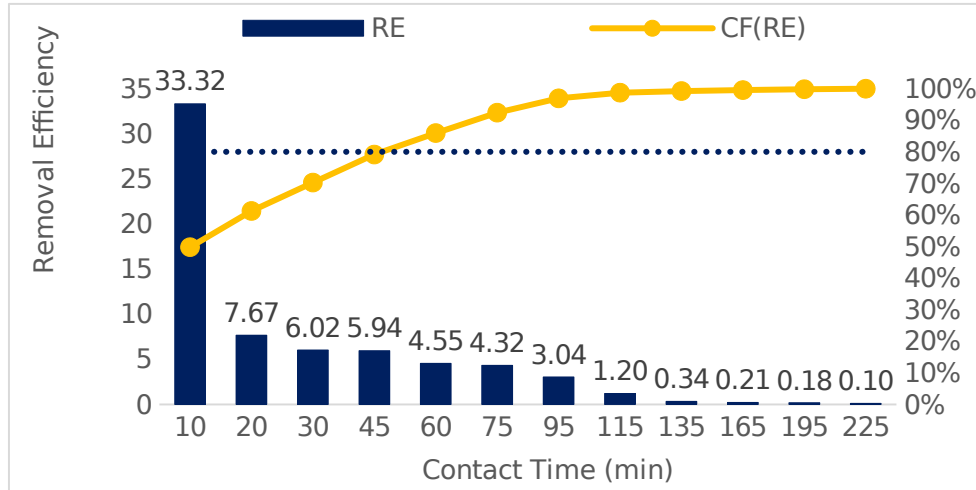


Figure 1: Pareto chart of (top) adsorption capacity (bottom) removal efficiency for the effect of contact time on CV dye.

3.3. Adsorption Kinetics

Several linear and nonlinear kinetic models were applied to investigate the adsorption kinetics of the experimental data of adsorption of crystal violet by FPB. Analyzing the kinetic parameters obtained from these models can provide valuable information for

estimating the adsorption rate and optimizing adsorption processes (Abbasi *et al.*, 2020; Patil *et al.*, 2020). The kinetic constants of each model studied in this inquiry are presented in Table 4-5 for linear and nonlinear appropriate.

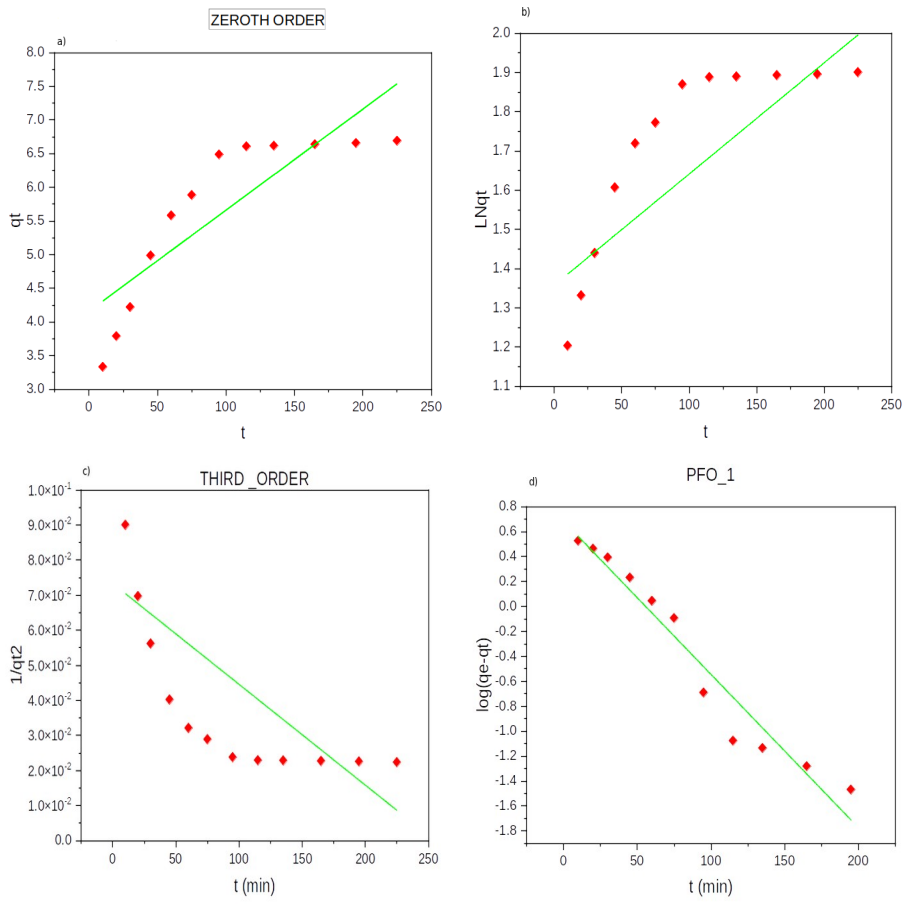
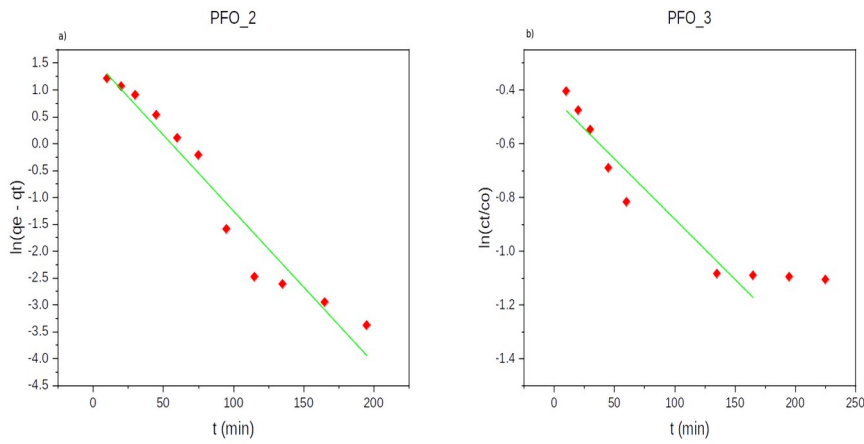


Figure 2: Graph of (a) Zeroth order (b) First Order (c) Second Order (d) Third Order Kinetic model.



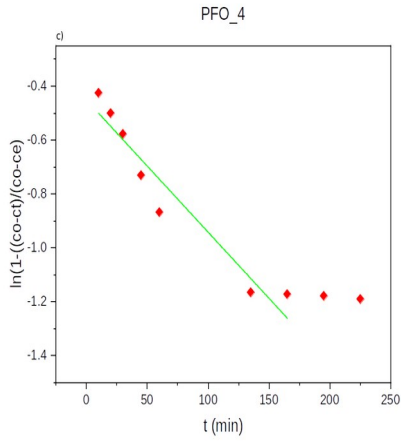
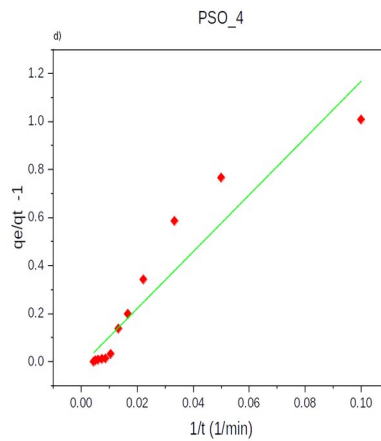
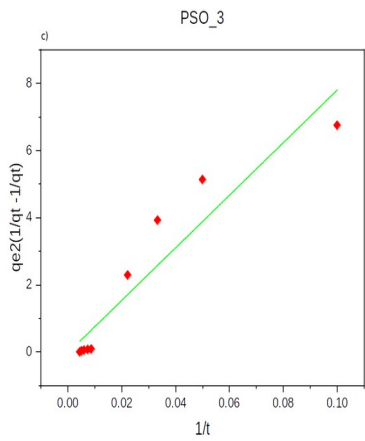
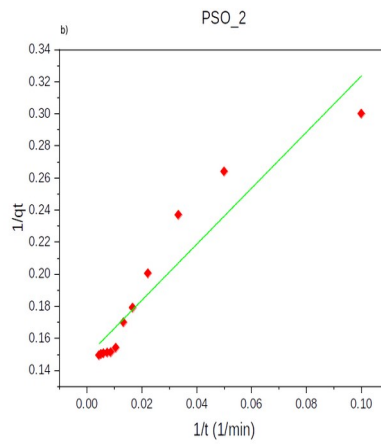
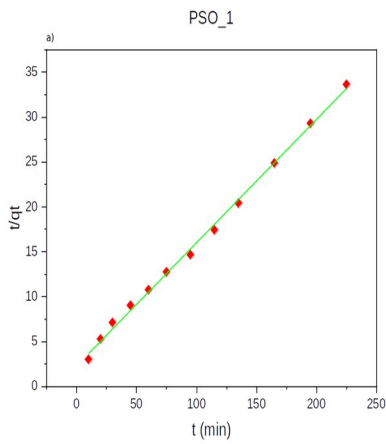
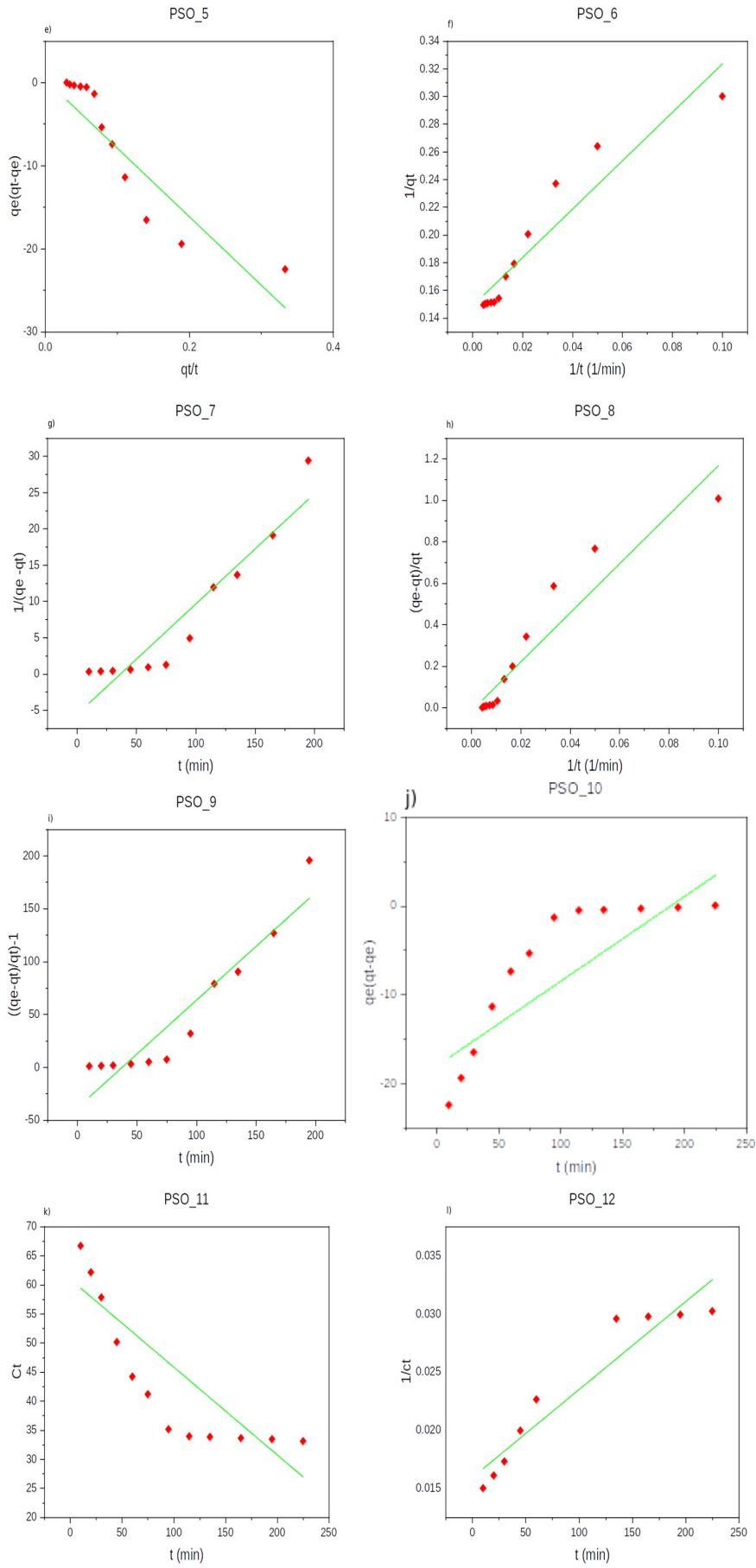


Figure 3: Graph of Pseudo First Order (a) Type 1, (b) Type 2, (c) Type 3





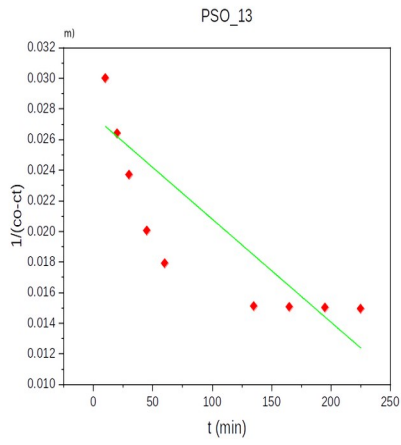


Figure 4: Graph of Pseudo Second Order (a) Type 1, (b) Type 2, (c) Type 3, (d) Type 4, (e) Type 5, (f) Type 6, (g) Type 7, (h) Type 8, (i) Type 9, (j) Type 10, (k) Type 11, (l) Type 12, (m) Type 13.

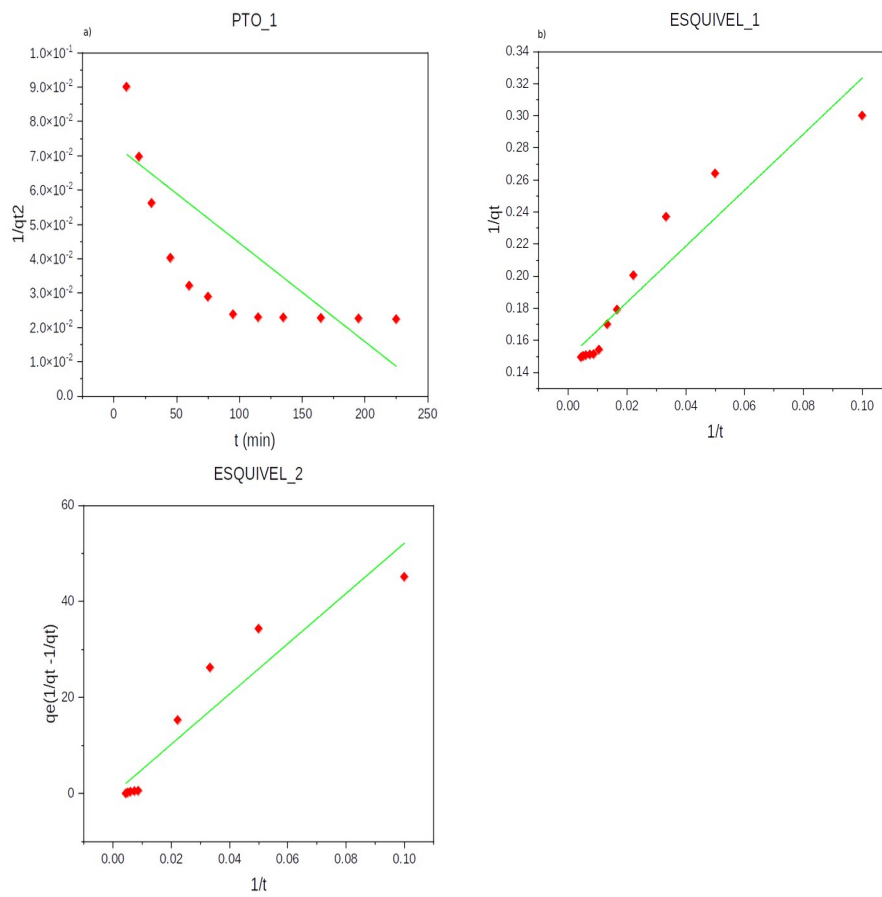


Figure 5: Graph of (a) Pseudo Third Order, (b) Esquivel Type 1, (c) Esquivel Type 2.

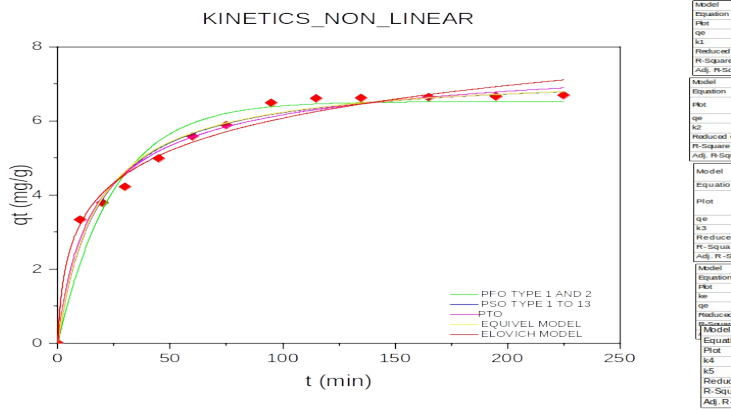


Figure 6: Graph of Non-linear Kinetic Models.

Table 4: Parameters of linear kinetic models.

Model	Parameter	Value	Model	Parameter	Value
Zeroth order	K_0	0.0150	PSO 7	K_2	0.1519
First order	K_0	0.0028	PSO 8	K_2	0.0126
Second order	K_0	-0.0006	PSO 9	K_2	1.0163
Third order	K_0	-0.0003	PSO 10	K_2	0.0956
PFO 1	K_1	0.0283	PSO 11	K_2	-0.1510
PFO 2	K_1	0.0283	PSO 12	K_2	7.56E-05
PFO 3	K_1	0.0045	PSO 13	K_2	-6.7E-05
PFO 4	K_1	0.0050	PTO	K_3	-2.8740
PSO 1	K_2	0.0598	Elovich 1	K_4	15.2137
PSO 2	K_2	0.0127		K_5	0.2327
PSO3	K_2	0.0128	Elovich 2	K_4	0.7961
PSO 4	K_2	0.0126		K_5	1.5877
PSO 5	K_2	0.0121	Esquivel 1	K_4	11.7437
PSO 6	K_2	0.0127	Esquivel 2	K_4	523.6213

Table 5: Parameters of non-linear kinetic models.

Kinetic Model	Parameter	Value
PFO 1	Q_E	6.5238
	K_1	0.0403
PSO 1	Q_E	7.3192
	K_2	0.0569
PTO	Q_E	8.4464
	K_3	0.0635
Elovich	K_4	1.4488
	K_5	0.7796
Esquivel	Q_E	7.3108
	K_5	0.5753

3.4. Error Analysis

As presented in Table 6, it is obvious that the non-linear Elovich kinetic model is the best

fitting model for the experimental data of the adsorption phenomenon studied with the lowest value of RSS, ARED, ARE, MPSED,

SSE, HYBRID, SAE=EABS, ARS, and Q = 100*ARS and the highest R², Adj. R² and (R-Value) values were found when modeling the experimental data using the pseudo-first-order model, pseudo-second-order, and pseudo-third-order model. The pseudo third-order model also displayed the lowest Reduced Chi-Sqr and RMSE values for the experimental data. The linear pseudo-second order type 2 proved to be the best fitting model for the adsorption experiment data as shown in Table 7 with the lowest ARED, MPSED, SSE, SAE=EABS, ARS, Q = 100*ARS, and MPSED values. The lowest value of RSS was attained by modeling pseudo-second-order model type 12 & 13 using the experimental data whereas the maximum values of R-Square, Adj. R² and Pearson's r were obtained by modeling Pseudo second-order kinetic model type 1. Esquivel Type 2 displayed the least value of ARE and SSE.

A swift comparison between linear and non-linear analyses was conducted to identify the most suitable error function(s) for each regression technique, employing the pseudo-second-order model as a case study. Our findings revealed that, in the context of

linear analysis, the regression coefficient (R²) attained the highest value (pseudo-second order type 1), making it the most acceptable error estimation tool for identifying the optimal kinetic model fit within a linear framework. Conversely, the other error functions (ARED, ARE, SAE, ARS, MPSED, Δq, SSE, MSPED, and HYBRID) exhibited superior suitability for non-linear analysis. It's important to note that the transition from non-linear to linear regression procedures introduces a shift in experimental error, presenting a unique challenge in error estimation that influences the validity of the chosen approach. Furthermore, the linear analysis technique implies that data points cluster around a Gaussian distribution, with error estimates remaining consistent at the equilibrium liquid-phase residual concentration value (X-axis) (Olaosebikan *et al.*, 2022). However, this behavior is inconsistent with equilibrium kinetic models, given their non-linear nature. Surprisingly, a non-linear regression approach mitigates such errors, rendering it the most suitable analytical method for obtaining more realistic isotherm parameters (Elmorsi *et al.*, 2022).

Table 6: Error analysis of the selected non-linear kinetic models.

Models	PFO 1	PSO 1	PTO	Elovich	Esquivel
R. Chi-Sqr	0.1863	0.0444	0.0558	0.0809	0.0823
R-Square	1.0000	1.0000	1.0000	0.9808	0.9804
Adj. R2	1.0000	1.0000	1.0000	0.9790	0.9786
RSS	2.0492	44.3303	5.7355	0.8895	0.9048
R-Value	1.0000	1.0000	1.0000	0.9903	0.9902
RMSE	0.4316	0.2108	0.4058	0.2844	0.2868
ARED	5.3477	0.1293	2.6956	1.8947	3.4189
ARE	0.0535	0.0129	0.0270	0.0189	0.0342
MPSED	0.1206	0.0237	0.0577	0.0387	0.0729
SSE	1.8788	0.1105	0.4518	0.2269	0.7189
HYBRID	0.0642	0.0195	0.0323	0.0253	0.0410
SAE=EABS	2.5371	0.5347	1.2482	0.9482	1.6139
ARS	0.1150	0.0303	0.0550	0.0350	0.0695
Q = 100*ARS	11.5034	3.0280	5.5042	3.5003	6.9474
MPSD	0.2273	0.1395	0.1103	0.0781	0.1390

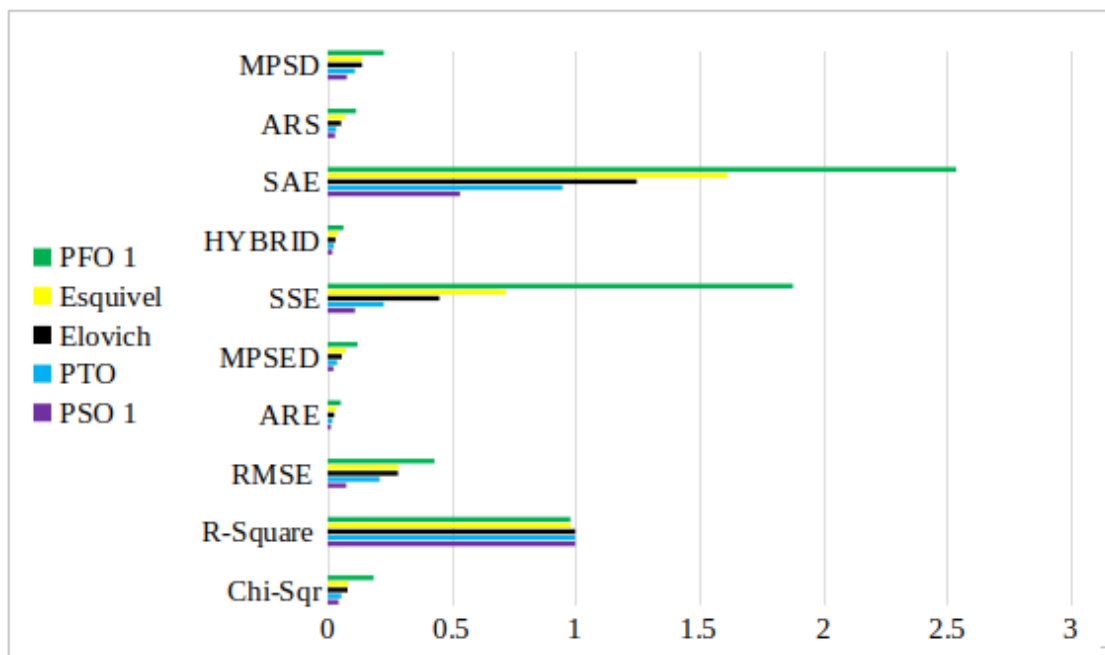


Figure 7: Plot of nonlinear kinetic error analysis.

Table 7: Error analysis of the selected linear kinetic models.

Kinetic Models	RSS	Pearson's r	R2	Adj. R2	ARED	ARE	MPSED	SSE	HYBRID	SAE=EABS	ARS	Q =100*ARS	MPSD
ZerOTH	4.632	0.8530	0.7276	0.7004	10.777	0.1078	0.1355	4.6316	0.1176	6.6411	0.1355	13.5484	0.2898
First	0.105	0.8948	0.8006	0.7673	12.324	0.1232	0.147	7.8734	0.1345	8.3549	0.147	14.7029	0.3487
Second	0.006	-0.8746	0.7649	0.7313	14.646	0.1465	0.1717	11.7751	0.1598	10.2293	0.1717	17.1702	0.4184
Third	0.001	-0.8838	0.7811	0.7446	14.646	0.1465	0.1717	11.7751	0.1598	10.2293	0.177	17.7021	0.4184
PFO 1	0.301	-0.9742	0.9491	0.9434	133.84	1.3384	1.9908	1921.15	1.4601	103.419	1.9908	199.079	5.1277
PFO 2	1.597	-0.9742	0.9491	0.9434	100.97	1.0098	1.8471	996.53	1.1016	58.2284	1.8471	184.714	4.1776
PFO 3	0.033	-0.9641	0.9294	0.9153	108.97	1.0977	1.7144	996.53	1.1566	58.8367	1.8714	184.737	4.7561
PFO 4	0.037	-0.9658	0.9328	0.9194	122.97	1.0098	1.8471	996.53	1.1016	58.2284	1.8471	188.714	4.1561
PSO 1	2.739	0.9987	0.9974	0.9971	4.7003	0.047	0.0014	0.9097	0.0513	2.5987	0.0014	0.1374	0.1114
PSO 2	0.003	0.9468	0.8965	0.8817	7.800	0.078	0.0061	0.2561	0.078	0.506	0.0061	0.610	0.0395
PSO3	5.700	0.9468	0.8965	0.8817	17.63	0.1763	0.0311	1.3078	0.1763	1.1436	0.0311	3.114	0.2016
PSO 4	0.134	0.9477	0.8981	0.8879	63.737	0.6374	1.0589	209.26	0.6953	32.2491	1.0589	105.887	2.1296
PSO 5	90.555	-0.9215	0.8492	0.8276	69.1724	0.6917	1.3086	252.97	0.7546	32.6196	1.3086	130.856	2.4935
PSO 6	0.003	0.9468	0.896	0.882	1.E+04	1.7E+02	2.4E+02	1.6E+07	1.5E+02	7.7E+03	2.4E+02	2.4E+04	5.3E+02
PSO 7	103.6	0.945	0.892	0.880	25.215	0.252	0.455	32.555	0.275	12.054	0.455	45.554	0.881
PSO 8	0.134	0.948	0.898	0.888	1.7E+04	1.7E+02	4.5E+02	6.8E+07	1.9E+02	1.1E+04	4.5E+02	4.5E+04	1.1E+03
PSO 9	4638	0.945	0.892	0.880	21.162	0.212	0.378	22.861	0.231	10.170	0.378	37.774	0.734
PSO 10	117.4	0.897	0.804	0.777	14.919	0.149	0.289	17.415	0.163	7.872	0.289	28.893	0.601
PSO 11	239.7	-0.915	0.837	0.814	14.986	0.192	0.289	17.454	0.127	7.723	0.289	28.930	0.604
PSO 12	0.000	0.952	0.906	0.892	19.919	0.492	0.889	17.154	0.175	7.831	0.293	28.759	0.643
PSO 13	0.000	-0.923	0.862	0.850	19.189	0.419	0.893	17.164	0.151	7.308	0.230	28.759	0.631
PTO	0.001	-0.884	0.781	0.745	40.438	0.404	0.654	94.482	0.441	21.319	0.654	65.439	1.373
Elovich-1	0.882	0.974	0.948	0.943	31.432	0.314	0.533	57.184	0.377	16.574	0.508	50.869	1.120
Elovich-2	0.882	0.974	0.948	0.943	31.232	0.332	0.352	57.358	0.319	16.427	0.569	50.876	1.118
Esquivel-1	0.003	0.947	0.896	0.882	5.420	0.054	0.064	0.748	0.067	1.679	0.064	6.379	0.129
Esquivel-2	255.20	0.9468	0.896	0.882	5.052	0.050	0.069	0.762	0.061	1.695	0.069	6.363	0.126

4. CONCLUSION

The efficacy of synthetic FPB for the removal of crystal violet dye from an aqueous solution was investigated in this research. Three parallel sets of trials were conducted using RSM based on CCD to investigate the effects of various operational elements and their relationships and then to determine the optimal circumstances. According to the statistical analysis results, a quadratic regression model may successfully grasp the experimental data. The Pareto chart was utilized to show the effects of time on the dye adsorption capacity and removal efficacy by the FPB adsorbent, and it was discovered that over 80% of the adsorption occurred during the first 45 minutes. Contour and surface plots demonstrated that increasing the time and decreasing the particle size of the FPB adsorbent resulted in the best removal performance of crystal violet dye. The surface plot also revealed that reducing particle size can result in the maximum adsorption capacity of crystal violet dye, as temperature was shown to be ineffective in the removal of crystal violet from wastewater.

5. ACKNOWLEDGMENTS

The authors acknowledge the Bioenvironmental Water Engineering Research Group (BEWERG) and the "Departments of Chemical Engineering Ladoke Akintola University of Technology (LAUTECH)" for the usage of their laboratories.

6. CONFLICT OF INTEREST

The authors uphold that there are no conflicts of interest related to the publication of this article.

7. REFERENCES

- Abbasi, F., Tavakkoli Yaraki, M., Farrokhnia, A., & Bamdad, M. (2020). Keratin nanoparticles obtained from human hair for removal of crystal violet from aqueous solution: Optimized by Taguchi method. *International Journal of Biological Macromolecules*, 143, 492-500. <https://doi.org/10.1016/j.ijbiomac.2019.12.065>
- Adekunbi, E. A., Babajide, J. O., Oloyede, H. O., Amoko, J. S., Obijole, O. A., & Oke, I. A. (2020). Evaluation of Microsoft Excel solver as a tool for adsorption kinetics determination. *Ife Journal of Science*, 21(3), 169. <https://doi.org/10.4314/ijfs.v21i3.14>
- Barber, S. T., Yin, J., Draper, K., & Trabold, T. A. (2018). Closing nutrient cycles with biochar- from filtration to fertilizer. *Journal of Cleaner Production*, 197, 1597-1606. <https://doi.org/10.1016/j.jclepro.2018.06.136>
- Batool, F., Akbar, J., Iqbal, S., Noreen, S., & Bukhari, S. N. A. (2018). Study of Isothermal, Kinetic, and Thermodynamic Parameters for Adsorption of Cadmium: An Overview of Linear and Nonlinear Approach and Error Analysis. *Bioinorganic Chemistry and Applications*, 2018, 1-11. <https://doi.org/10.1155/2018/3463724>
- Benmaamar et al. (2017). A batch study of adsorption equilibrium and kinetic for methylene blue onto synthesized zeolite. <http://www.jmaterenvironsci.com/>, 8(2), 539-550.
- Chahinez, H.-O., Abdelkader, O., Leila, Y., & Tran, H. N. (2020). One-stage preparation of palm petiole-derived biochar: Characterization and application for adsorption of crystal violet dye in water. *Environmental Technology & Innovation*, 19, 100872. <https://doi.org/10.1016/j.eti.2020.100872>
- Çoruh, S., & Geyikçi, F. (2012). Adsorption of copper (II) ions on montmorillonite and sepiolite clays: Equilibrium and kinetic studies. *Desalination and Water Treatment*, 45(1-3), 351-360. <https://doi.org/10.1080/19443994.2012.692058>
- Elmorsi, R. R., Abou-El-Sherbini, K. S., Shehab El-Dein, W. A., & Lotfy, H. R. (2022). Activated eco-waste of Posidonia oceanica rhizome as a potential adsorbent of methylene blue from saline water. *Biomass Conversion and Biorefinery*. <https://doi.org/10.1007/s13399-022-02709-5>
- Hami, H., Abbas, R., Jasim, A., Abdul Abass, D., Abed, M. A., & Maryoosh, A. A. (2019). Kinetics study of Removal Doxycycline drug from aqueous solution using Aluminum Oxide surface. *Egyptian Journal of Chemistry*, 0(0), 0-0. <https://doi.org/10.21608/ejchem.2019.5499.1483>
- Lairini, S.E, Mahtal, K, Miyah, Y, Tanji, K, Guissi, S, Boumchita, S, & Zerrouq F. (n.d.). Adsorption of Crystal violet from aqueous solution by using potato peels (*Solanum tuberosum*): Equilibrium and kinetic studies. *Journal of Materials and Environmental Sciences*, 8(9), 3252-3261.
- Loulidi, I., Boukhliji, F., Ouchabi, M., Amar, A., Jabri, M., Kali, A., Chraibi, S., Hadey, C., & Aziz, F. (2020). Adsorption of Crystal Violet onto an Agricultural Waste Residue: Kinetics, Isotherm, Thermodynamics, and Mechanism of Adsorption. *The Scientific World Journal*, 2020, 1-9. <https://doi.org/10.1155/2020/5873521>
- Olafadehan, O.A., (2021). Fundamentals of Adsorption Processes, ISBN: 978-620-3-30705-4, LAP Lambert Academic Publishing, Omni-Scriptum DUE GmbH.
- Olaosebikan, A. O., Victor, E. B., Kehinde, O. A., & Adebukola, M. B. (2022). Isotherms, kinetic and thermodynamic studies of methylene blue adsorption on chitosan flakes derived from African giant snail shell. *African Journal of Environmental Science and Technology*, 16(1), 37-70. <https://doi.org/10.5897/AJEST2021.3065>
- Patil, S. R., Sutar, S. S., & Jadhav, J. P. (2020). Sorption of crystal violet from aqueous solution using live roots of *Eichhornia crassipes*: Kinetic, isotherm, phyto and cyto-genotoxicity studies. *Environmental Technology & Innovation*, 18, 100648. <https://doi.org/10.1016/j.eti.2020.100648>
- Popoola, L. T. (2019). Characterization and adsorptive behaviour of snail shell-rice husk (SS-RH) calcined particles (CPs) towards cationic dye. *Heliyon*, 5(1), e01153. <https://doi.org/10.1016/j.heliyon.2019.e01153>

Akinyemi, A. G. et al., (2024). JOTCSB, 7(2), 105-122.

Rosly, N. Z., Abdullah, A. H., Ahmad Kamarudin, M., Ashari, S. E., & Alang Ahmad, S. A. (2021). Adsorption of Methylene Blue Dye by Calix[6]Arene-Modified Lead Sulphide (Pbs): Optimisation Using Response Surface Methodology. *International Journal of Environmental Research and Public Health*, 18(2), 397. <https://doi.org/10.3390/ijerph18020397>

Shojaei, S., Ahmadi, J., Davoodabadi Farahani, M., Mehdizadeh, B. and Pirkamali, M.R. (2019). Removal of crystal violet using nanozeolite-x from aqueous solution: Central composite design optimization study. *Journal of Water and Environmental Nanotechnology*, 4(1). <https://doi.org/10.22090/jwent.2019.01.004>

Sivarajasekar, N., & Baskar, R. (2019). Adsorption of Basic Magenta II onto H2SO4 activated immature Gossypium hirsutum seeds: Kinetics, isotherms, mass transfer, thermodynamics and process design. *Arabian Journal of Chemistry*, 12(7), 1322–1337. <https://doi.org/10.1016/j.arabjc.2014.10.040>

Vyavahare, G., Jadhav, P., Jadhav, J., Patil, R., Aware, C., Patil, D., Gophane, A., Yang, Y.-H., & Gurav, R. (2019). Strategies for crystal violet dye sorption on biochar derived from mango leaves and evaluation of residual dye toxicity. *Journal of Cleaner Production*, 207, 296–305. <https://doi.org/10.1016/j.jclepro.2018.09.193>

Zamouche, M., Habib, A., Saaidia, K., & Bencheikh Lehocine, M. (2020). Batch mode for adsorption of crystal violet by cedar cone forest waste. *SN Applied Sciences*, 2(2), 198. <https://doi.org/10.1007/s42452-020-1976-0>

Zarei, M., A., Niaei D., Salari A., & Khataee A. (2010). Application of Response Surface Methodology for Optimisation of Peroxi-Coagulation of Textile Dye Solution Using Carbon Nanotube-PTFE Cathode. *Journal Hazard Material*, 173, 544–551.

